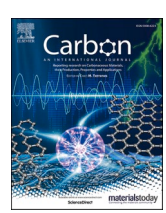


Contents lists available at ScienceDirect

Carbon

journal homepage: www.elsevier.com/locate/carbon





2D graphene oxide and MXene nanosheets at carbon fiber surfaces

Katarina Adstedt^a, Madeline L. Buxton^a, Luke C. Henderson^b, David J. Hayne^c, Dhriti Nepal^c, Yury Gogotsi^d, Vladimir V. Tsukruk^{a,*}

- ^a School of Materials Science and Engineering, Georgia Institute of Technology, Atlanta, GA, 30332, United States
- ^b Institute for Frontier Materials, Deakin University, Geelong, Vic., 3216, Australia
- ^c Air Force Research Lab, Materials and Manufacturing Directorate, 2941 Hobson Way, WPAFB, Ohio, 45433, United States
- d A. J. Drexel Nanomaterials Institute and Department of Materials Science and Engineering, Drexel University, Philadelphia, PA, 19104, United States

ARTICLE INFO

Keywords: Carbon fiber composites 2D nanomaterials MXene Graphene oxide Carbon fiber surface modifications

ABSTRACT

Carbon fibers, which are known for their high strength to weight ratio and thermal and chemical stability, are key components in advanced structural composites. Controlling the fiber-matrix interface is key to achieving required physical performance. Functional two-dimensional (2D) materials that can conformally coat the fiber surface facilitate interface and interphase engineering for enhanced mechanical properties and added functionalities. Understanding how 2D flakes bond, integrate, and perform at carbon fiber interfaces is key to developing multifunctional high-strength composites. In this study, we focus on the surface interactions of graphene oxide (GO) and $Ti_3C_2T_x$ MXene nanoflakes at the surface of low-tension carbon fibers with and without amine functionalization by in-depth multimode scanning probe microscopy. We suggest that beyond strengthening the interfaces, GO and MXene provide efficient charge transfer with MXene also adding conductivity to the fiber surface, extending potential applications of composites to broad areas including structural supercapacitors and battery cooling/packaging materials. GO and MXene modified fibers not only create opportunities for increased interfacial adhesion in composites via increased surface roughness, but also act as anchors for bonding, energy dissipation, charge transport, and local interface stiffening.

1. Introduction

Carbon fiber composites, known for their high strength to weight ratio, mechanical integrity, and high thermal and chemical stability are key structural composites in the defense, aerospace, sporting, and energy industries [1–4]. A pivotal component to the performance of carbon fiber in composites is the interphase, which demonstrates a gradient of properties cderived from stiff carbon fibers and the relatively weaker polymer matrix [1,2,5–7]. These nanoscale interfacial regions exhibit critical mechanical failure due to poor adhesion between the fiber and the matrix, mismatch between the thermal expansion coefficients, poor interdiffusion, and/or poor energy transfer [1,8,9]. Tailoring the surface functional groups on the carbon fiber surface, adding interphase components, or altering the carbon fiber morphology have been shown to strengthen the interphase and reduce the chance of critical failure.

Recent methods of modifying carbon fiber surfaces heavily rely on carbonaceous nanomaterials, such as carbon black, carbon nanotubes (CNT), and graphene-based derivatives, due to their high dispersibility and hybridization [1,10,11]. These modified carbon fiber composites demonstrate increased flexural strength/modulus, impact strength, interfacial shear strength, and young's modulus [12]. Furthermore, many studies showed enhancement in modified composite performance, varying from ~ 0.25 wt% to 1 wt%, after which a clear drop in performance was observed [11-13]. Efforts to improve interfacial bonding are focused on strong adhesion; however, while these modifications increase interfacial strength, they might be coupled with a decrease in toughness as energy absorption is limited [9]. To achieve synergistic strengthening and toughening of carbon fiber composites, more ductile interfacial layers are incorporated [14]. These multi-layers typically result in core-sheath structures, where ultrathin two-dimensional (2D) materials encapsulate a carbon fiber surface, providing the opportunity for energy dissipation over carbon fiber microgrooves [15].

Amongst modern 2D nanomaterial additions, graphene oxide (GO) (and its derivatives) offer chemical tunability, high specific surface area, high Young's modulus, and high thermal conductivity, while being fairly low-cost and scalable [16,17]. Similarly, MXenes, "up and coming

E-mail address: vladimir@mse.gatech.edu (V.V. Tsukruk).

^{*} Corresponding author.

new age materials," are scalable 2D nanomaterials with high energy storage capabilities, high surface area, high negative surface charges, and hydrophilicity [17-19]. They exceed graphene oxide in strength, modulus and conductivity, while having similar dispersibility in water and polar solvents. MXenes, or early transition metal carbides and nitrides with numerous surface functional groups (-F, -O, -OH) and transition metal layers (Ti, V, Nb, Mo), have conductivity upwards of 20, $000\,\mathrm{S\,cm}^{-1}$, which outperforms graphene and its derivatives [18,20,21]. They are becoming increasingly researched due to these impressive physical properties [17,22]. 2D nanomaterials are commonly integrated on the carbon fiber surface via chemical vapor deposition, coating, chemical grafting, solvothermal treatment or electrophoretic deposition [13,23-26]. Deposition of MXenes and GO nanoflakes from solution can significantly increase fiber surface energy, wettability, and surface roughness [24-26]. Increases in interfacial adhesion result in greater interfacial and interlaminar shear strength, tensile strength, and flexural strength [23,26]. Ti₃C₂T_x MXene is the most commonly used MXene variation due to its composition including earth abundant elements, high conductivity, excellent strength and environmental stability. It has been applied to glass fibers [27] and stress transfer from polymer matrix to MXene was recently demonstrated using Raman spectroscopy [28].

It is known that integrating GO and Ti₃C₂T_r to carbon fiber surfaces can increase wettability, surface energy, and surface roughness to increase interfacial adhesion and composite interfacial shear strength, yet many studies exploring GO and Ti₃C₂T_x interactions with carbon fibers ignore the nanoscale interactions [13,25]. While numerous studies have investigated the macroscopic and microscopic properties, few have considered individual 2D nanoflakes at the carbon fiber surfaces [2,29]. In this study, we focus on the surface interactions of GO and MXene nanoflakes at the carbon fiber surfaces by in-depth multimode scanning probe microscopy. Previously, multi-length scale exploration of carbon fiber surfaces demonstrated that low tension fibers (LT), or carbon fibers processed at a tension of 1800 cN during carbonization, and amine functionalized low tension fibers (LT-NH) have low fractal dimensions, varied microscale surface roughness, and low nanoscale surface roughness [31]. The LT and LT-NH fibers were selected for his work due to their unique surface chemistry and varied surfaces with similar performances.

2. Methods

2.1. Synthesis

2.1.1. Materials

Carbon fibers were manufactured (carbonized in-line and electrolytically oxidized) per previous publications and used un-sized [30,31]. The low-tension fiber processing and subsequent amine functionalization were conducted as previously outlined [31,32]. ${\rm Ti}_3{\rm C}_2{\rm T}_x$ MXenes were synthesized as reported in recent publications [22].

2.1.2. $Ti_3C_2T_x$ MXene preparation

 $Ti_3C_2T_x$ MXene was synthesized according to previous publications via the Minimally Intensive Layer Delamination (MILD) method [22,33, 34]. 2D titanium carbide microscopic MXene flakes were extracted from a concentrated sediment containing multi-layer MXene and residual MAX phase, and dispersed in ultra-pure deionized water, hand-shaken, and centrifuged for 1 h at 3500 rpm. The initial colloidal solution contained 0.0042 wt% MXene after preparation. Two separate MXene solutions were prepared by centrifuging 5 μL of 0.0042 wt% MXene solution at 3500 rpm and extracting the supernatant, until 0.5 wt% concentration of MXene in water was reached.

2.1.3. Graphene oxide (GO) preparation

Graphene oxide was prepared from 325 mesh graphite following the Hummers' method [35,36]. Initial wt% after GO preparation was 0.63 wt%. The solution was diluted to 0.5 wt% by adding ultra-pure

deionized water and sonicating for 10 min to disperse [20].

2.1.4. Carbon fiber -2D composite manufacturing

Carbon fiber – GO composites and carbon fiber – MXene composites were prepared using dip coating method [2,37]. Each compound was prepared into two separate 0.5 wt% suspensions with ultra-pure deionized water, in which the LT and LT-NH carbon fibers were separately submerged for 12 h. At the 12-h mark, the carbon fibers were extracted from the respective solutions and rinsed with ultra-pure deionized water [9,38]. The fibers were dried under vacuum for 48 h and mounted onto carbon tape on a silicon wafer for characterization.

2.2. Characterization

2.2.1. X-ray photoelectron spectroscopy (XPS)

The measurements were conducted using a Thermo K-Alpha XPS with Al K_{α} radiation (hn=1486~eV). For the survey scans, three scan were collected with a dwell time of 50 ms and a 1.0 eV step size. For the high-resolution scans, 10 scans were collected with a dwell time of 50 ms and a 0.1 eV step size [39,40]. XPS data analysis was performed using CasaXPS. A Shirley background correction was performed. All components were calibrated based on the C1s peak for sp [2]-hybridized carbon atoms at 284.5 eV, and peak fitting was performed using symmetric Gaussian-Lorentzian profiles. Three major constraints were imposed during deconvolution. Specifically, all component binding energies were constrained to \pm 0.5 eV and the full width half maximum (FWHM) values of each component were constrained. Finally, all Ti 2p3/2 and 2p1/2 components were constrained to an area ratio of 2:1 [38,39].

2.2.2. Atomic force microscopy (AFM) and scanning modes

Multi-length scale characterization was conducted using a Bruker Dimension Icon AFM [2]. The composites' surface topography and morphology were evaluated using high-resolution AFM (HR-AFM). HR-AFM was conducted using a ScanAsyst scanning probe (tip radius, r=2 nm; resonant frequency, $f_0=70$ kHz, spring constant, k=0.4 Nm $^{-1}$). Scans were collected with a scan rate of 0.40 Hz, at 3 $\mu m \times 3 \mu m$ and 500 nm \times 500 nm, all at 512 \times 512 samples/line. This results in a highest nominal resolution of 1 nm at 500 nm scan sizes [31,41]. For all scans, at least three separate surface locations were scanned.

A minimum of 5 individual 2D nanoflakes were imaged per sample type. A minimum of 6 nanoflakes were imaged for each specimen. All measurements and quantification of root mean square (RMS) surface roughness, R_q , and average mean surface roughness, R_a , were conducted using Nanoscope 2.0. Surface roughness and structures were further evaluated using power spectral density (PSD) analysis [42–44]. The produced PSD plots are 2D Isotropic functions of the x and y directions.

Fractal dimensions were calculated using the equation: $D = \frac{\left(\frac{\log(PSD)}{\log(\omega)} - 5\right)}{2}$

Physical properties (compression modulus, energy dissipation, adhesion, chemical composition, and electrostatic potential) were evaluated with multimode scanning probe microscopy (SPM) via quantitative nanomechanical mapping (QNM), Kelvin probe force microscopy (KPFM), and Nano-IR AFM [47–49]. QNM was conducted at a scan rate of 0.35 Hz, with 512×512 samples/line, at a constant applied force of 400 nN. The scanning probe used for these mechanical measurements, specifically modulus, was a PDNSP-HS diamond tip (r=40 nm; $f_0=50$ kHz; k=350.1 Nm $^{-1}$). The scanning force applied was 400 nN, which results in a mean indentation of 2 nm. The indentation force used in 15 μ N, resulting in an Hertzian indentation of ~5 nm [2,29].

KPFM measures the changes in local surface electrostatic potential and can be used to calculate the work function of materials or understand the charge distribution on the sample surface [50]. We employed Peak Force KPFM (PF-KPFM), or Peak Force tapping combined with frequency modulation KPFM. Frequency modulation KPFM relies on oscillating AC voltage at low frequencies with a single scan pass, relying

on long-range electrostatic effects [51]. A PFQNE-AL probe was used for the PF-KPFM scans (r=5 nm; $f_0=300$ kHz; k=0.8 Nm $^{-1}$). The scans were conducted at a scan rate of 0.5 Hz, at 512×512 samples/line, at 3 μ m, with an applied voltage of 4.00 V at a lift height of 110 nm above the sample surface. An input $I_{\rm gain}$ and $P_{\rm gain}$ of 10 and 20 were used, respectively. A minimum of two nominally identical samples, three locations each, were characterized for each combination of independent variables [50]. The work function of the tip was calibrated on an Au standard sample [52].

Nanoscale infrared spectroscopy experiments for chemical mapping were conducted on an AFM-IR instrument, nanoIR3, from Bruker [2]. A quantum cascade laser (QCL) was used as an IR source covering the wavelength from 800 $\rm cm^{-1}$ to 1800 $\rm cm^{-1}$. Ten background spectra were collected and then averaged to subtract the background influence on the IR signal. All spectra and maps were generated using contact mode with mode NIR2 probe for NanoIR2, model PR-EX-nIR2-10 (Anasys Instruments Inc., Santa Barbara, USA) with a resonance frequency of 13 ± 4 kHz, a spring constant of 0.007–0.4 N m $^{-1}$ and a tip radius of 40 nm. Scans were collected at a scan rate of 0.3 Hz, with 512 \times 512 samples/line, at 1720 and 1010 cm $^{-1}$ wavenumbers.

2.2.3. Scanning electron microscopy (SEM)

SEM was conducted on a Hitachi-SU8230, with a $10.00~\mathrm{kV}$ accelerating voltage. Modified fibers were mounted on an aluminum stub with a conductive tape.

2.2.4. ImageJ analysis

Analysis was performed using ImageJ software. Five AFM topographical images for each of the fibers were analyzed to determine the average percentage of surface coverage of the 2D additions.

3. Results and discussions

To reveal how the underlying surfaces may affect 2D materials, we studied GO grafted to both the LT and LT-NH fiber and MXene grafted to the LT and LT-NH fibers, resulting in four samples of modified carbon fibers total with: 1) GO grafted to LT fibers (LT-GO), 2) GO grafted to LT-NH fibers (LT-NH-GO), 3) MXenes grafted to LT fibers (LT-MX), and 4) MXene grafted to LT-NH fibers (LT-NH-MX).

The GO and MXene nanosheets exhibit similar 2D morphology and properties (Fig. 1, Table S1) (see Supporting Information). The GO nanoflakes are $2.4\pm0.5~\mu m$ across with an average height of 0.9 ± 0.3 nm, typical GO nanoflake dimensions [13,17,26,53]. Similarly, the MXenes are $1.6\pm0.6~\mu m$ wide and $3.2\pm1.1~\mu m$ long, with an average height of 1.3 ± 0.2 nm, typical of MXenes materials reported to date [17, 20,22,23].

The measured nanosheet thickness for both 2D nanomaterials is slightly higher than nominal thickness, likely a result of tip-sample interactions, and trapped surface adsorbates [17]. The surface charge of the GO is increased by the number of carboxyl and hydroxyl functional groups on the surface of the flakes [54]. As seen in the chemical structures given in Fig. 1, MX flakes also have oxygen-containing functional groups on the surface, but fewer than that of GO leading to the difference in surface potential of the individual flakes. Both GO and MXene surfaces possess low surface roughness, $R_{\rm q}$, of 1.1 \pm 0.4 nm and 0.9 \pm 0.2 nm, respectively, due to the presence of wrinkles caused by drying over

1000 nm² area. Their similar topography extends to their fractal dimensions, 2.0, characteristic of true 2D materials [45].

3.1. Composition and surface topography

XPS survey spectra of carbon fibers after deposition of 2D flakes confirm the coating process and reveal the presence of C 1s, O 1s, N 1s, and Ti 2p peaks (Fig. 2, S1). The survey scan confirms functionalization with the amine functional groups on the LT fibers. GO containing samples have similar compositions to pure GO, so ratios of C to O on LT-GO and LT-NH-GO fit with the literature [55]. Furthermore, the presence of the Ti 2p peak confirms successful MXene deposition on the fiber surface [56]. The presence of Na can be attributed to the NaNO $_3$ used to prepare GO via the Hummers' method.

The primary regions of interest to understand how Ti₃C₂T_x MXenes and GO integrate at carbon fiber surfaces are C 1s and Ti 2p. These peaks are deconvoluted in Fig. 2. The GO nanoflakes are primarily bonding to the carbon fiber surface through C-C, C-O, and COO bonds while MXene flakes are confirmed via the presence of C-Ti-T_x bonds. Some contribution from the fiber can be assumed in the XPS data of the composite due to the partial surface coverage from the 2D materials. However, there is noticeable additional contribution from both the GO and MX showing their deposition. For the LT-GO, LT-NH-MX samples, higher presence of oxygen from the GO compared to the LT carbon fiber is found (Table S2). The LT-MX and LT-NH-MX samples have higher presence of both oxygen, found in the terminating groups on the flakes, and the addition of titanium. Additionally, there is no contribution within N1s or Ti2p and therefore no evidence of the C-Ti-Tx bonds in the base fiber. Detailed positions, full width at half max and composition are included in Table S2

On local Nano-IR AFM spectra, only characteristic peaks below 2000 cm⁻¹ are observed due to a limited wavenumber range accessible (Fig. S2a) [57,58]. There are peaks at 1760, 1695, and 1680 cm⁻¹ for the LT and LT-NH pristine fibers, corresponding to the C=O stretching vibrations [56]. The LT-NH control fiber also demonstrates peaks at 1470 and 1430 cm⁻¹, which correspond to C-N stretching, 1380 cm⁻¹ which corresponds to C-C stretching [55,56]. It is important to note that these peaks are strongly diminished for the GO and MXene modified fibers, especially for the MXene modifications (Fig. S2b). Moreover, the LT-GO and LT-NH-GO modified fibers demonstrate peak shifts for C-C bonds, to 1320 cm⁻¹, which can be attributed to the bonding between GO and the underlying carbon fibers [56].

In contrast, the Nano-IR spectra for MXene flakes show strongly diminished peaks at 1060 cm⁻¹ indicating increased hydrogen bonding for self-assembled MXenes on the amine modified carbon fibers, with carboxyl groups on CF from O rich groups on MXene [37]. The reduced intensity of peaks for LT-MXene composites show C=O bonds were weakened, and O-H bonds between carboxyl groups on the surface and hydroxyl of MXene established [55]. The peak intensity increases (1740 cm⁻¹, C=O stretching), further indicating strong bonding between the LT-NH fiber and MXenes nanosheets.

Overall, it seems that the LT-NH fiber is best suited for MXene additives for potentially strongly bonded composites. Electrostatic attraction between the negatively charges MXene flakes [59] and positively charged amine on the fiber surface should also be considered. MXenes can interact with carbon fiber surfaces via hydrogen bonding and

Table 1Surface topography properties for modified carbon fibers with added GO and MXene components.

Base Fiber	2D component	2D Coating Height on Fiber [nm]	2D Coating Surface Coverage [%]	RMS Nano-roughness, $R_{\rm q}$ [nm]	Nano-Fractal Dimension	RMS Microrough-ness, R_q [nm]	Micro-Fractal Dimension
LT	GO	2.4 ± 0.4	38 ± 19	12 ± 3	2.47	35 ± 11	2.5
LT-NH	GO	2.1 ± 0.7	45 ± 15	14 ± 4	2.49	31 ± 10	2.4
LT	$Ti_3C_2T_x$	2.9 ± 0.9	32 ± 7	25 ± 9	2.49	32 ± 5	2.5
LT-NH	$Ti_3C_2T_x$	3.8 ± 1.5	44 ± 12	23 ± 9	2.49	39 ± 15	2.4

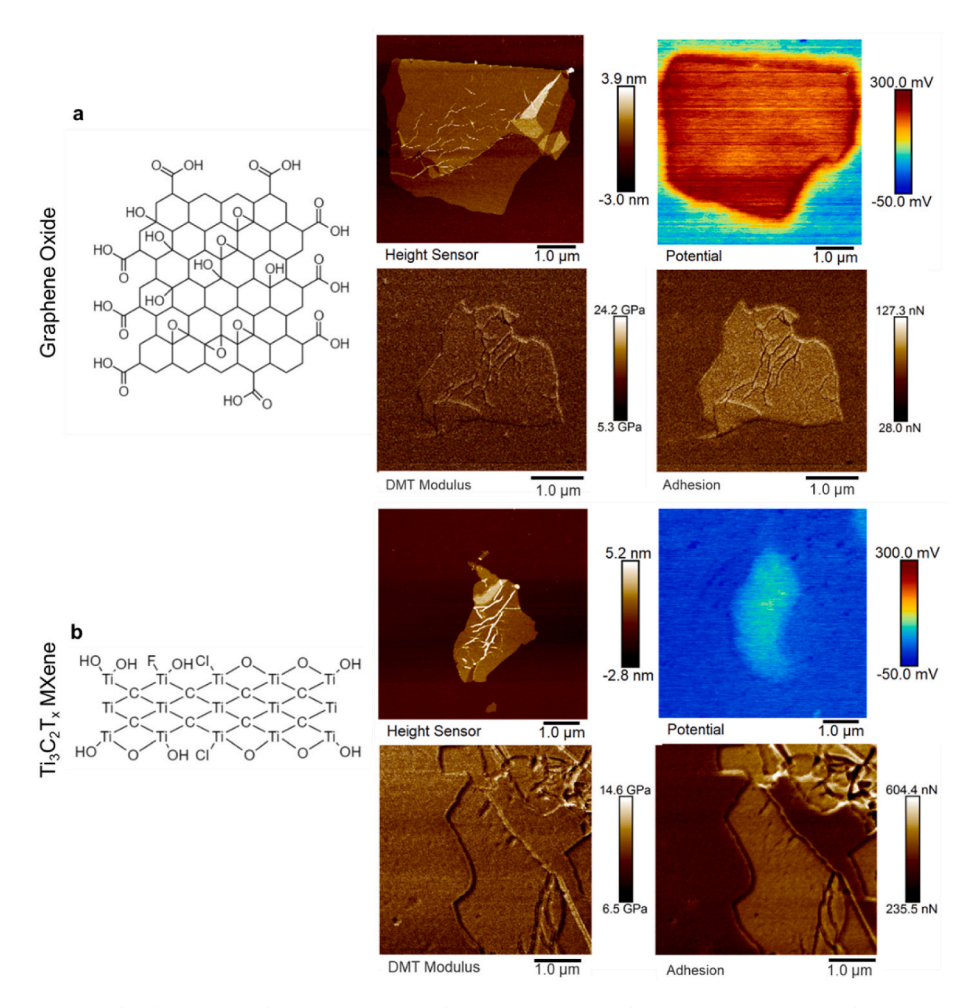


Fig. 1. Characteristics of 2D materials additive to carbon fibers a) GO and b) $Ti_3C_2T_x$: chemical structure, AFM topography, QNM measured DMT modulus and adhesion, and electrostatic potential mapped with KPFM. (A colour version of this figure can be viewed online.)

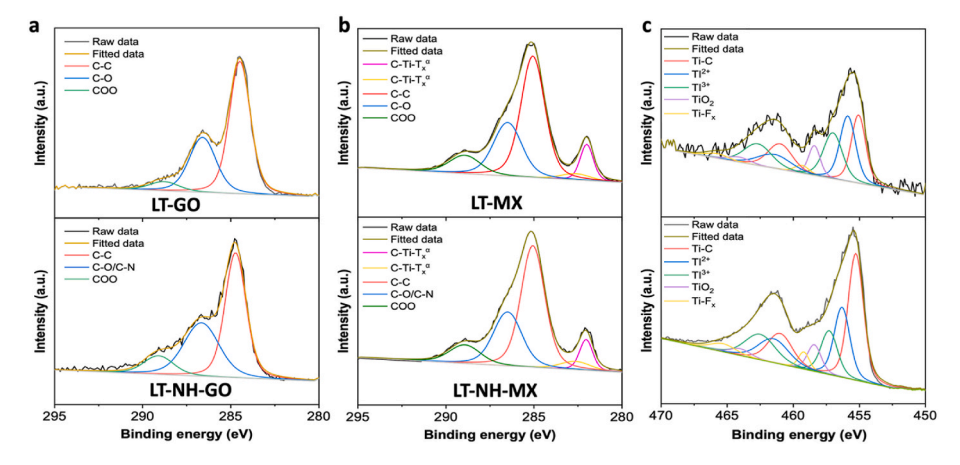


Fig. 2. XPS peak deconvolution of the C 1s for a) GO modified samples and b) MXene modified samples. c) Ti 2p peak deconvolution for MXene containing samples. (A colour version of this figure can be viewed online.)

electrostatic interactions because of their negative zeta potential, approaching –40 mV at neutral pH, and hydrophilicity [57]. Removal of adsorbed water upon drying at elevated temperatures may produce covalent bonds linking the fiber and the flake; however, the predominant bonding mechanisms between the carbon fibers and MXenes are hydrogen bonding, van der Waals, and electrostatic interactions [57].

SEM images of the four samples demonstrate that the 2D

nanomaterials are locally attached to the fiber surface (Fig. S3). All four modified carbon fibers exhibit the presence of crumpled 2D nanoflakes on the surface, enveloping the fiber grooves (Fig. S3). However, the wrapping of 2D nanoflakes is highly dependent upon their type and surface functionalities.

The apparent surface coverage with GO flakes, as calculated from AFM images differs for different fibers, is 38% on the LT fibers, whereas

it is 45% on the LT-NH fiber. Example calculations are provided in Fig. S4. In this study, the MXene exhibited a 32% and 44% surface coverage at the macroscale, for LT and LT-NH fibers, respectively (Table 1, Fig. S4). Based on these observations, MXenes integrate with carbon fibers by amine coordination to the terminated with abundant functional groups Ti, creating a uniform MXene sheath [36]. The partial coverage of the GO and ${\rm Ti}_3{\rm C}_2{\rm T}_x$ on the carbon fibers can be attributed to the low weight percentage of the solutions during assembly because full coverage is typically achieved by absorption from concentrated suspension (around 1 mg/mL) [37].

As seen from comparison of Fig. 3a and b and Fig. 3c and d, the GO nanoflakes and their aggregates cover the fiber surface as individual flakes, and then the nanoflakes combine to create a cohesive "wrapping" or sheath on the fiber micro-grooves. In contrast, the MXene is present on the carbon fiber microfibrils mostly as individual nanoflakes. In some instances, the MXene nanoflakes stack upon each other within the fiber microgrooves creating rough surfaces with crumbled coating (Fig. 3 d, h).

3.1.1. Surface properties of GO integrated at fiber surfaces

The non-uniform distribution of GO nanoflakes at the surface is not unusual for GO modified carbon fibers. Indeed, depending on the flake size, GO may 1) lie flat in large layered patterns, 2) lie flat in a sparse, random order, or 3) edge bond, with lifted edges along the fiber surface [13]. In this study, we primarily see GO arrange itself in large, layered patterns on the LT base fiber, with occasional lifting of the GO nanoflake edges off of the carbon fiber surface (Fig. S3a). In contrast, there is little to no lifting of the GO on the LT-NH fiber. Instead, the GO nanoflakes arrange themselves in seemingly sparse, random orders as the GO is more strongly bonded to the surface. Wrinkling of GO sheets on the fiber surface is a desired characteristic as it increases the interfacial interlocking in carbon fiber composites [13,24,25]. Some regions of GO exhibit agglomeration due to strong π - π interlayer stacking [1].

As seen in high resolution AFM scans of individual flakes, GO can wrinkle (Fig. 3e) or fold over itself (Fig. 3f). The wrinkled structure is a direct result of structural defects formed during oxidation of the GO, while the disordered carbons and oxygen-containing functional groups initiate bonding between GO layers and nanoflakes to result in folded microscale structures with the wrinkling or crumpled texture [26]. The carboxyl and hydroxyl surface groups in LT-GO react to create strong covalent bonding, while the amine functional group reacts in LT-NH-GO with GO to create C-N bonds by epoxide reaction [26].

As known from our previous study, the base LT fibers have high microscale surface roughness, at 20.5 ± 0.2 nm, with fractal dimensions

of 2.4, which decrease to 2.2 at the nano-scale, where surface roughness is 1.2 \pm 0.2 nm [31]. The LT-NH fibers, however, have a microscale surface roughness of 11.1 \pm 1.8 nm and nano-scale surface roughness of 1.6 \pm 0.3 nm [31]. As we observed, the addition of GO sheets increases the fiber surface roughness, evidenced by a 70% and 180% increase in $R_{\rm q}$ due to the presence of crumpled GO flakes (Table 1). Here, and below, the surface characteristics for different surface coverages have been obtained by analyzing multiple selected surface areas for multiple images, averaging corresponding characteristics, and deriving standard deviations.

Interfacial interactions of GO flakes primarily rely on van der Waals forces, hydrogen bonding, and π - π bonds to adsorb onto the fiber surface, whereas the amine modified LT fiber adsorb to the fiber surface primarily through electrostatic interactions and hydrogen-bonding. The hierarchical structure, in a core-sheath model, initiates increased surface roughness, which, in turn, increases surface energy by increasing the effective bonding area [13,36]. The oxygen functional groups on the GO surface increase the polarity of the carbon fiber, facilitating the effective bonding. Similarly, the O-H groups on carbon fiber surface interact with GO nanoflakes, resulting in strong hydrogen bonds. Thus, with the increased surface roughness, the GO modified carbon fibers are expected to have increased interfacial adhesion in prospective composites.

3.1.2. Properties of carbon fiber surfaces with MXene coating

The LT-MXene of fiber surfaces demonstrate a 56% increase in surface roughness from the LT fiber and a much higher, 250%, increase in surface roughness from the base LT-NH fiber (Table 1). The increased corrugation at the fiber surface is likely due to the uptake in carboxyl and hydroxyl groups as well as hydrogen bonds that originate due to the negatively charged ${\rm Ti}_3{\rm C}_2{\rm T}_x$ -OH nanoparticles [55]. Moreover, the true difference in topography of fibers modified with MXenes is at the nano-scale. Pure LT fibers exhibit chain-like arrays of surface dimples, as discussed in our previous publication [31]. In contrast, grafted multilayered ${\rm Ti}_3{\rm C}_2{\rm T}_x$ flakes can be compactly overlapped, demonstrating folds and wrinkles within the nanoflakes, as the MXenes can readily bond with other nanoflakes [36].

Indeed, there is unreacted nitrogen on the surface of the fibers as seen from XPS (Fig. 2). This is typically in pyridine-type structures, which also possess the capability to donate electrons into the d-orbital of the titanium in the MXene and may, at least to a small extent, contribute to the uptake of MXenes on the bare surface of the fibers. MXenes' strong polarity increases surface adherence with acid-functionalized carbon fibers – forms strong interfacial connections [1]. The abundant functional groups at the MXene surfaces (-F, -OH, =O), create potential

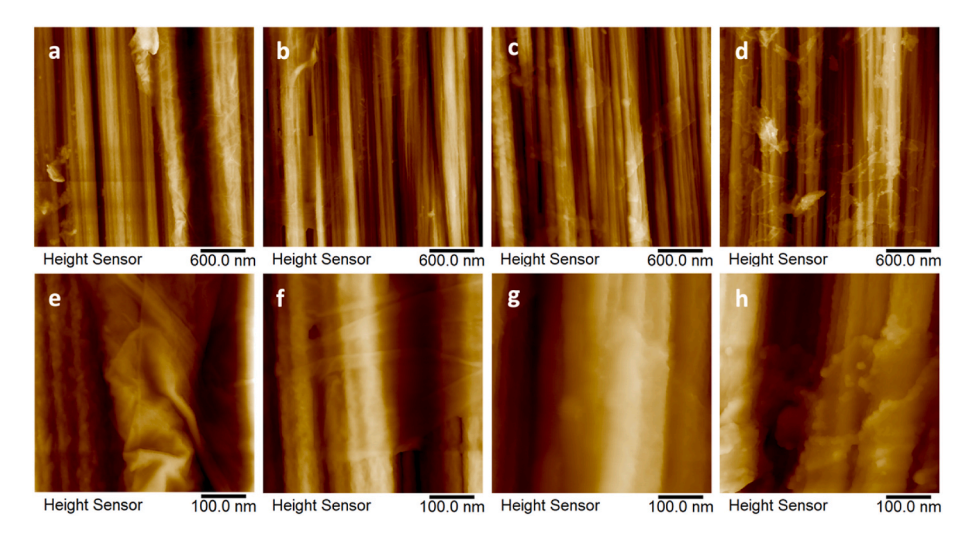


Fig. 3. AFM scans of a) GO grafted on LT fibers, b) GO grafted on LT-NH fibers, c) MXene grafted on LT fibers and d) MXene grafted on LT-NH fibers. Corresponding high-resolution scans at 500 nm for each fiber are included in e)-h), respectively. (A colour version of this figure can be viewed online.)

opportunities for the nanoflakes to non-covalently bond at the carbon fiber surface [36].

3.1.3. Comparing GO and MXene at carbon fiber surfaces

As we discussed above, topographical analysis reveals how GO and MXene differ in structure and the influence of the underlying base fiber on the 2D nanomaterials bonding capabilities. The randomly dispersed nanoflakes are easily identified. The clear increase in surface roughness is evidenced by the increase in R_0 from the base LT and LT-NH fibers to the GO and MXene modified carbon fibers. Generally, adding either GO or MXene leads to increased fiber corrugation or roughness, which can inhibit inter-laminar shearing by increasing the friction forces between composite materials [1,26]. Although surface roughness on the scale of tens of nanometers may not directly contribute to mechanical interlocking in interphase adhesion, it increases the total contact area, which initiates efficient molecular interactions and strengthens the interphase [29]. The increased surface roughness for the LT-NH-MXene interfaces is sustained down to the nano-scale, indicating the composite would demonstrate the highest interphase strength via increased surface roughness of the four composites in this study. It is worth noting that power spectral density (PSD) analysis characterizes the surface topography concurrently at multiple length scales (Fig. 4).

This PSD analysis shows that consistent fractal dimensions increase across the spatial length scales (Table 1) [43]. The elevated level of PSD signal demonstrates consistently increasing roughness at all spatial scales tested (Fig. 4). This corresponds with the quantitative data and indicates that these two composite combinations are geared towards increased interdigitation in prospective composites.

Next, high resolution AFM images show features of flake bridging grooves and covering ridges (Fig. 5). Yet it is their ability to remain unwrinkled or folded, unlike the GO, to create a flat, rough, and uniform surface at the nanoscale. Higher fractal dimensions indicate higher tortuosity of the fiber surface. The roughness and tortuosity, or corrugated surface, of the carbon fiber composites can be easily seen in 3D depictions of the scans (Fig. 5).

Though previously speculated from the 2D images that the GO and MXene nanoflakes bridge the gaps between microgrooves and begin to fill them in, the 3D images reveal how the nanoflakes mold to the microgrooves rather than directly bridge them [52]. Although the 2D nanomaterials were grafted at the same weight percentage, the GO and MXenes differ greatly in how they bond and incorporate at the fiber surface with GO primarily deposited in thin nanoflakes. However, both types of nanoflakes attempt to bridge valleys between the longitudinal striations on selected locations.

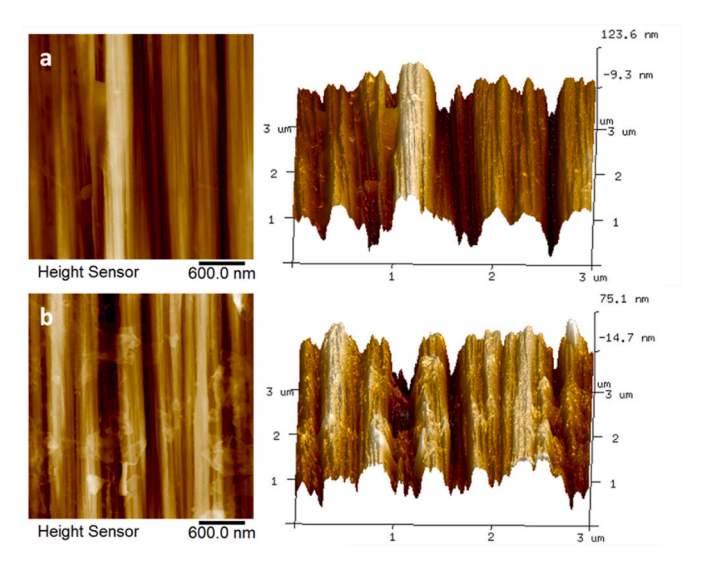


Fig. 5. 3D AFM images of nanoflake integration on the LT-NH fiber surface modified with a) graphene oxide nanosheets and b) MXene nanosheets. (A colour version of this figure can be viewed online.)

3.2. Physical surface properties

3.2.1. Nanomechanical mapping

Here, we discuss QNM mapping of the nanomechanical properties (Fig. 6) [13,60].

Adhesion from QNM measurement specifically reflects the chemical interaction and physical bonding between the scanning probe tip and the targeted sample [58]. The strength of the interface is a factor of the work of adhesion [61]. Interfacial adhesion can be physical (intermolecular forces), chemical (chemical bonding), or mechanical (interlocking and entanglement of polymer chains with the fiber structural defects) [62]. The differences in adhesion between the composite surfaces can be attributed to either the surface properties (such as roughness or chemical heterogeneities) as they interact with the scan tip or to the interaction forces between the sample and the tip [58]. The primary chemical interactions at carbon fiber composite surfaces range in strength, from van der Waals forces and electrostatics, to capillary forces, steric forces, or chemical bonds [58].

The presence of GO and MXene flakes results in a drastic decrease in the adhesion from the original base fibers (Fig. 6, Table 2, Table S4). The GO modified fibers demonstrate a 37.5% and 17% decrease in surface adhesion when GO is grafted to the LT and LT-NH fibers, respectively. In contrast, the LT-MX composite is the only MXene grafted fiber to

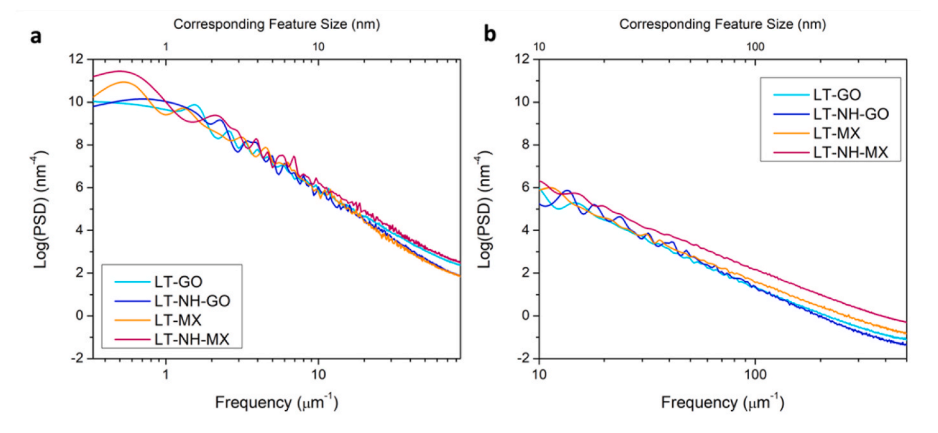


Fig. 4. Power spectral density plots at the a) microscale and b) nano-scale, demonstrating spatial-frequency distribution in the 2D-fiber composite surfaces. (A colour version of this figure can be viewed online.)

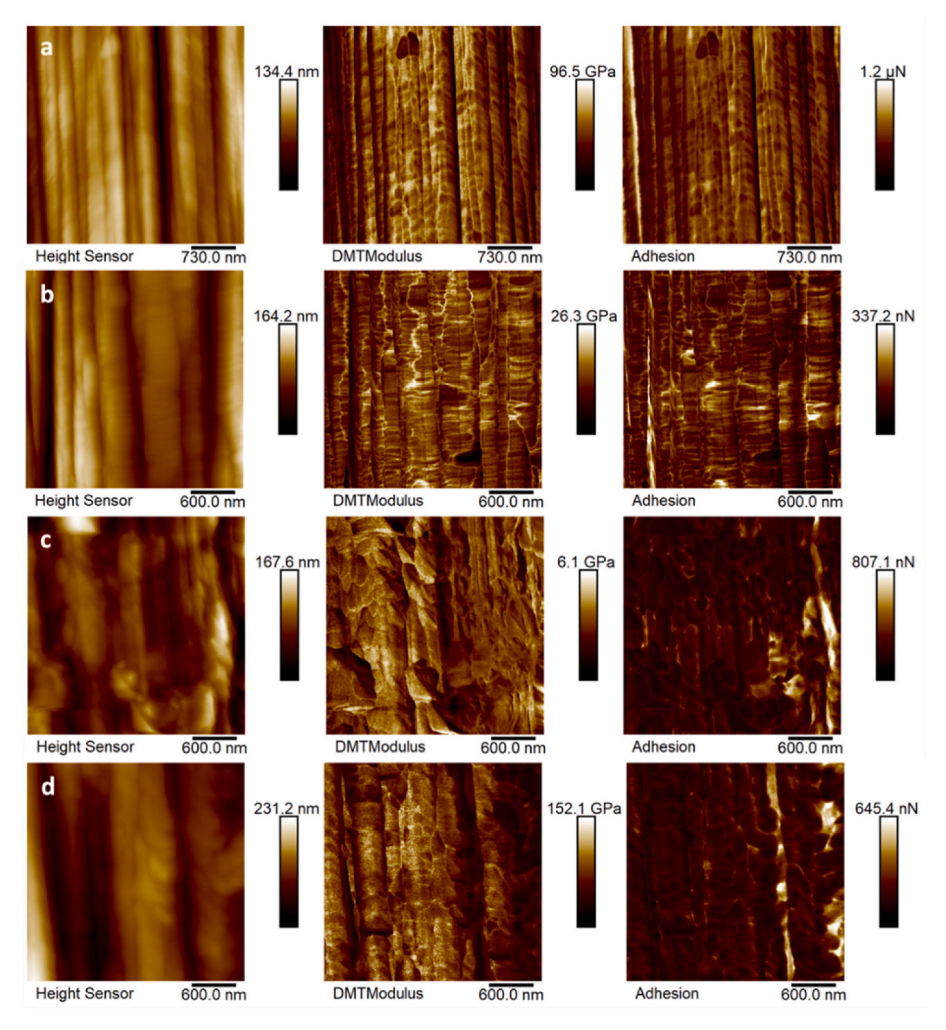


Fig. 6. Nanomechanical mappings of the topography, DMT modulus, adhesion, and energy dissipation for different modified fiber surfaces: a) LT-GO, b) LT-NH-GO, c) LT-MXene, and d) LT-NH-MXene fibers. (A colour version of this figure can be viewed online.)

Table 2Mechanical and electrostatic properties of carbon fiber surfaces coated with different 2D flakes.

Base Fiber	2D components	DMT Modulus [GPa]	Adhesion [nN]	Energy Dissipation [J], 10 ⁻¹⁵	Surface Potential [mV]
LT	GO	15 ± 1	75 ± 28	0.6 ± 0.2	47 ± 21
LT- NH	GO	8 ± 6	58 ± 18	0.6 ± 0.1	41 ± 8
LT	$Ti_3C_2T_x$	8 ± 5	53 ± 25	0.2 ± 0.1	64 ± 13
LT- NH	$Ti_3C_2T_x$	19 ± 3	70 ± 10	0.3 ± 0.1	43 ± 3

demonstrate a change in surface adhesion, demonstrating a 55% decrease with the integration of MXene. The tip-sample adhesion for individual MXene flakes is 41 \pm 11 nN, whereas the LT-NH fiber tip-sample adhesion is 70 \pm 20 nN, which would initially indicate that the LT-NH fiber was not thoroughly integrated with MXene at its surface. We can conclude that the MXenes are integrated at the surface nonuniformly, with spacing between MXene nanoflakes allowing for the tip to interact with the underlying carbon fiber [20]. In contrast, the larger GO nanoflakes facilitate stronger interfacial interactions because of increased interfacial area with crumpled and wrinkled flakes of these large flakes.

The differences in adhesion at the surface of the LT-GO vs. LT-NH-GO and LT-MXene vs. LT-NH-MXene, can be attributed to the effects of the

underlying carbon fiber surface and the respective 2D nanomaterials methods of integration at the surface. The GO modified fibers demonstrate a 22% decrease in adhesion when grafted to the LT-NH fiber instead of the LT fiber, whereas the MXene grafted fibers exhibit 32% increase in adhesion. Both GO and MXene are stacking, evidenced by their bi- and tri-layer thickness on the carbon fibers (Table 1). However, due to the coordination effect and strong bonding between the N- and Tigroups on amine modified carbon fibers and MXenes, the LT-NH-MXene interfaces exhibit the highest level of bonding and highly resistant shearing ability.

The DMT modulus mapping shows the stiffer and softer areas partially compromised by local topography (Fig. 6) [2,63]. Overall, we observe a decrease in the apparent modulus of the modified fibers down to 8-20 GPa range (Table S3) [64,65]. When there is strong hydrogen bonding between the fiber and the 2D nanomaterial, there is nearly a 2x increase in modulus at the composite surface. Increase in Young's modulus but decrease in tensile strength with increasing nanomaterial interphase filler is a result of the fiber brittle behavior which decreases strength but increases stiffness [66]. As known, increased surface roughness leads to increased interfacial strength via increased specific surface area [1,58]. The LT-MXene composite slightly defies expectations in terms of modulus due to its high surface roughness, but this can be attributed to poor interfacial adhesion between the pure LT carbon fiber and Ti₃C₂T_x [67]. The LT-NH-MXene composite is expected to have the highest mechanical interfacial adhesion due to strong electrostatic and vdW interactions, which increase mechanical

interlocking and shearing resistance [1]. Further, we suggest that this pairing would initiate the highest chemical adhesion because the N- and Ti- have increased affinity [1].

3.2.2. Surface electrostatic potential

Examples of surface potential and the corresponding surface topography obtained with KPFM mode for the four modified fibers are shown in Fig. 7. The GO modified fibers, LT-GO and LT-NH-GO, have lower contact potential difference (CPD), or surface potential, than the MXene modified fibers (Table 2). The electrostatic forces measured during KPFM scanning, between the sample and the conductive probe, is expressed as:

$$F_{sp} = -\frac{1}{2} \frac{\partial C}{\partial z} \Delta V^2$$

where $\partial C/\partial z$ is the capacitance gradient between the sample and scanning probe, ΔV is the contact potential difference between the sample and probe, in which z is the distance between the probe and sample [68]. The CPD on the sample surface is 4.00 V, as $V_{\text{CPD}} = V_{\text{DC}}$ in frequency

modulation KPFM in efforts to keep the amplitude zero [66].

Further examining histograms is vital to fully understanding the performance of the modified carbon fibers (Fig. 8). The histograms, with representative Abbot plots, demonstrate where the GO-fiber and MXenefiber composites behave similarly in property distribution, while also highlighting where the 2D materials differ, regardless of the underlying base fiber surface. The use of MXenes at the carbon fiber surface, as compared to GO nanoflakes, rapidly increases the composites capability of conducting electron transport and other electrical performances. MXene and graphene oxide nanosheets, when standing freely on flat silicon substrates, exhibit surface potentials of 24 \pm 5 and 16 \pm 2 mV, respectively (Table S2). The local surface potential of MX composites increases by 30-40 mV, whereas the GO-fiber composites, LT-GO and LT-NH-GO, demonstrate less positive surface potentials with a max of 40 mV (Fig. 8). Both LT-NH modified composites demonstrate narrower surface potential that indicates few chemical functional groups on the fiber surface, with a uniform density distribution of surface charges [50].

In terms of physical adhesion and DMT modulus the different

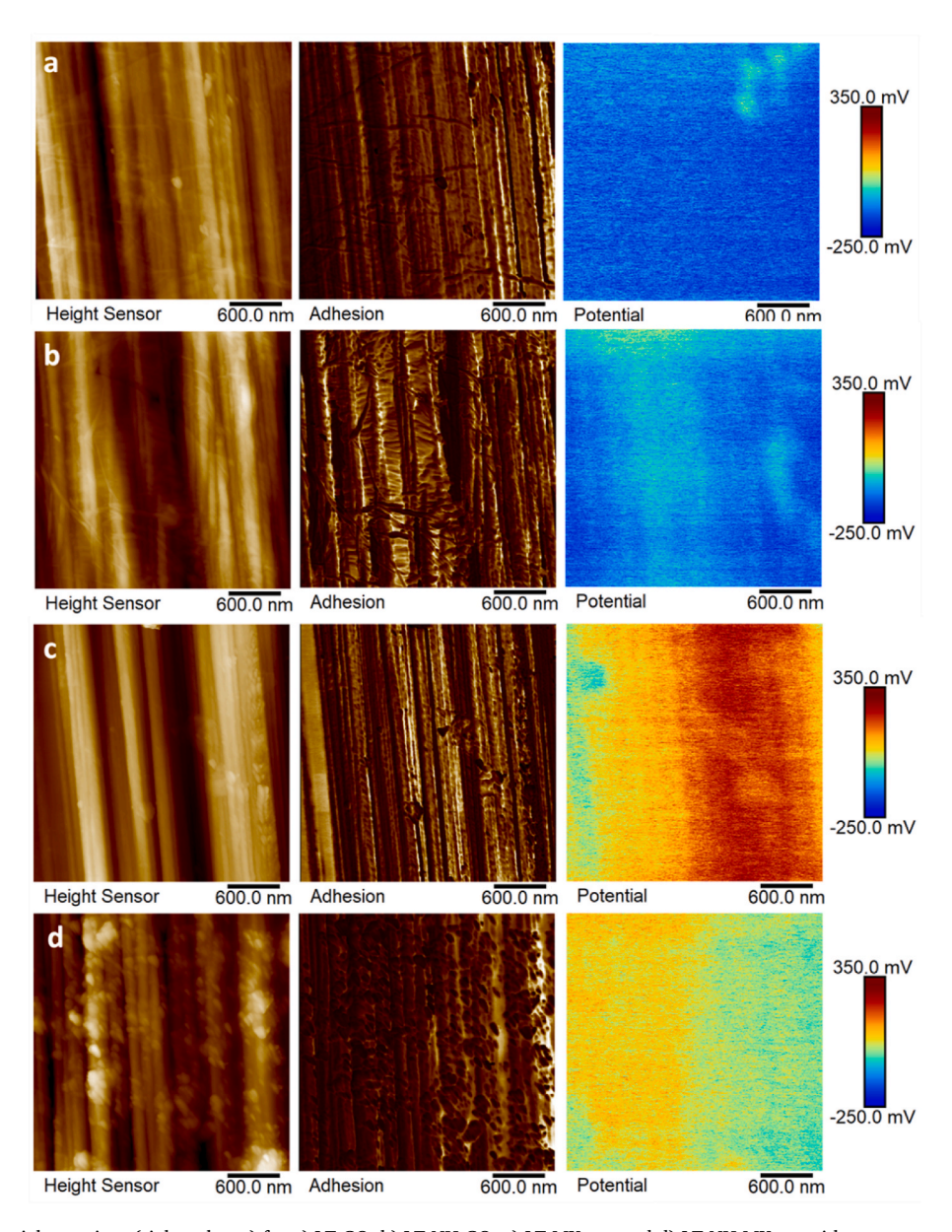


Fig. 7. Electrostatic potential mappings (right column) for a) LT-GO, b) LT-NH-GO, c) LT-MXene, and d) LT-NH-MXene with concurrent topography and adhesion mappings. (A colour version of this figure can be viewed online.)

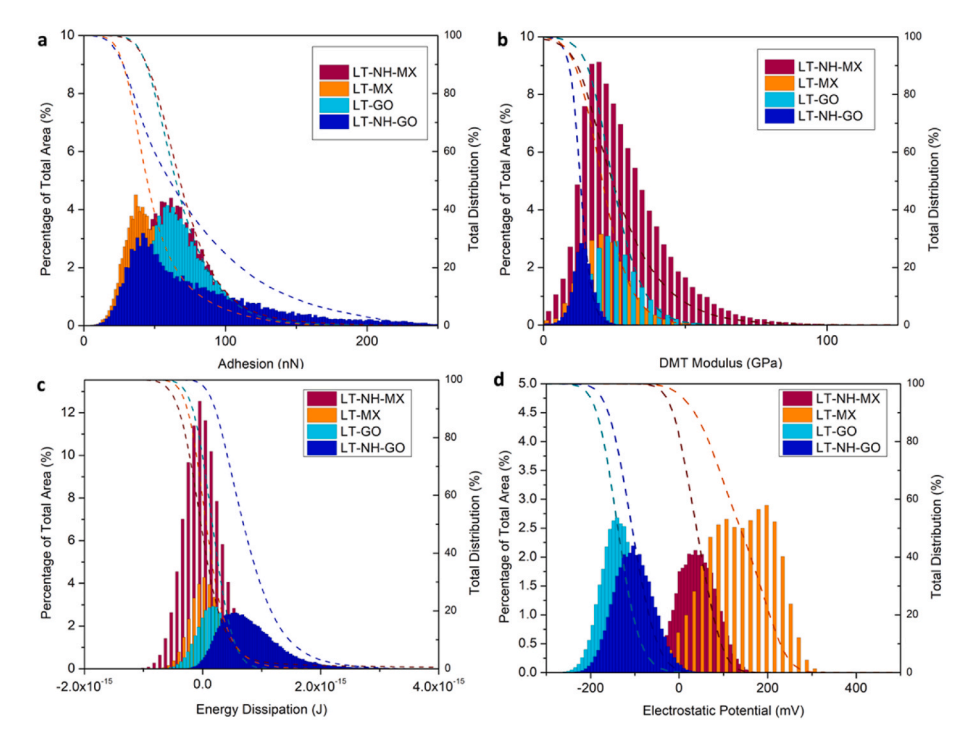


Fig. 8. Histograms representing the distribution of a) adhesion, b) DMT modulus, c) dissipation and d) surface potential for LT-GO, LT-NH-GO, LT-MXene, and LT-NH-MXene modified carbon fiber surfaces. (A colour version of this figure can be viewed online).

modified fiber surfaces perform similarly (Fig. 8a and b). The LT-GO and LT-NH-GO composite surfaces both demonstrate higher energy dissipation by a factor of three. Graphene oxide nanoflakes exhibit an energy dissipation of $0.20\pm0.01\cdot10^{-15}$ J, whereas MXenes exhibit an energy dissipation of $0.29\pm0.05\cdot10^{-15}$ J (Table S2, Fig. 1). On the other hand, the more negative and lower surface potential of the GO modified fibers indicates that flakes have a lower work function than MXenes [69]. The surface potential only decreased 13% for GO-fiber composites, while the dissipation and adhesion similarly only decreased by a few percent between the LT-GO and LT-NH-GO composites. This implies that the GO modified fibers have higher charge transfer from the sample to the substrate and, understandably, a higher oxygen content on the surface which allows for more oxygen vacancies, allowing more electrons to act as donors [50,51,70].

4. Conclusions

This study showed that the fiber surface functionalization with ultrathin 2D materials plays a significant role in their surface appearance, topography, roughness, fractal nature, electrostatic potential, and local mechanics. Both GO and MXene nanosheets modify surface properties including increased surface roughness, enhanced surface functionalization for bonding, and potential for charge transfer. Adding GO nanosheets to the surfaces of LT fibers more significantly improves properties whereas adding MXene to LT-NH fibers best enhances the overall performance. We observed strong bonding and good surface integration with as-received carbon fibers for the GO nanoflakes. MXenes, on the other hand, demonstrate stronger bonding with LT-NH over LT due to the presence of amino groups. This is explained by the electrostatic attraction of negatively charged MXene flakes to the positively charged amine on the surface. While there was not a significant difference in topography, we observed a near doubling in mechanical strength and electrical conductivity in the modified fiber surfaces. A combination of electrostatic and vdW bonds with a possible contribution from noncovalent bonds, like electrostatic forces, van der Waals, and hydrogen bonds, can lead to optimal interphase performance [9]. Evaluating the energy dissipation at the nanoscale reveals how the addition of 2D

nanomaterials at the carbon fiber surface modifies the dissipation capabilities and their distribution across the fiber surface. Notably, the MXene composites lose any repeating structures or units at the nano-scale, while the GO composites do not. The MXene flakes are randomly orientated on the fiber surface and do not mask the fiber microgrooves at the macro-scale, probably due to their smaller size and higher stiffness than GO. The energy dissipation is nearly twice as high for GO modified fibers compared to MXene modified fibers. Due to the nature of their integration and nanostructures morphology, GO bridge envelops more of the fiber local sites of high energy dissipation. However, compared to the pure carbon fibers, there is a drastic decrease in the mechanical dissipation for all four modified surfaces by a factor of three.

The nanoscale characterization of the interphase between the CF and the 2D materials elucidate ways to strengthen advanced carbon fiber-reinforced composites for future applications. Characterization of interphase regions with the hierarchical topographical, mechanical, and charging surface distribution provides insight into how the materials can be tailored to improve overall mechanical performance and functional attributes in further use for composite reinforcement [71]. Overall, we suggest that GO and MXene-modified fibers create opportunities for increased interfacial adhesion in corresponding composites due to the increased surface roughness with asperities and crumples regions acting as anchors for bonding, energy dissipation, and local interface stiffening.

Furthermore, it is important to note that, beyond strengthening the interfaces due to the unique mechanical properties of GO and MXene additives, both 2D materials have efficient charge transfer abilities that modify significantly surface potential and charging ability of interfaces with dielectric matrix [15–18]. MXene nanosheets also add surface-anchored metallic conductivity ability to the fiber surface and significantly increases fiber electrostatic surface potential. The composite, therefore, takes advantage of the added functionalization of the 2D additions while maintaining the fiber's strength, weight, and performance. Considering the combination of these enhanced surface roughness, and modified electrical and mechanical properties, we suggest that by integrating multifunctional 2D nanomaterials at the carbon fiber surface, the applications of the composite can be extended to

high-performance aerospace applications with efficient charge dissipation and trapping, light weight and volume battery cooling/packaging materials for electric vehicles, and arrested crack propagation at fiber-matrix interfaces [26,72].

CRediT authorship contribution statement

Katarina Adstedt: sample preparation, experimental work, manuscript writing, Writing – original draft. Madeline L. Buxton: some experimental support, help with manuscript writing, Writing – original draft. Luke C. Henderson: fibers manufacturing, manuscript writing, Writing – original draft. David J. Hayne: Fiber manufacturing. Dhriti Nepal: research planning, manuscript writing. Yury Gogotsi: MXene manufacturing, manuscript writing, Writing – original draft. Vladimir V. Tsukruk: research planning, manuscript writing, Writing – original draft.

Declaration of competing interest

The authors declare the following financial interests/personal relationships which may be considered as potential competing interests: Yu. Gogotsi reports financial support was provided by National Science Foundation. V. Tsukruk reports financial support was provided by Air Force Research Laboratory. D. Nepal reports financial support was provided by AFOSR. L. Henderson reports financial support was provided by Australian Research Council.

Acknowledgements

We'd like to acknowledge Dr. Christine Hatter (Drexel University) for preparing the MXenes. This research was supported by Air Force Research Laboratory (AFRL) grant FA8650-18-F-5828 PO30-00695 and the Australian Research Council (DP220100130P). Y.G. acknowledges support from the US National Science Foundation (grant DMR-2041050) for collaboration with AFRL and D. N. acknowledges support from Air Force Office of Scientific Research (22RXCOR014).

Appendix A. Supplementary data

Supplementary data to this article can be found online at https://doi.org/10.1016/j.carbon.2022.11.028.

References

- [1] P. Banerjee, R. Raj, S. Kumar, S. Bose, Tunable chemistry at the interface and self-healing towards improving structural properties of carbon fiber laminates: a critical review, Nanoscale Adv. 3 (2021) 5745–5776.
- [2] L. Liu, C. Jia, J. He, F. Zhao, D. Fan, I. Xing, M. Wang, F. Wang, Z. Jiang, Y. Huang, Interfacial characterization, control and modification of carbon fiber reinforced polymer composites, Compos. Sci. Technol. 121 (2015) 56–72.
- [3] M. Sharma, S. Gao, E. Mäder, H. Sharma, L.Y. Wei, J. Bijwe, Carbon fiber surfaces and composite interfaces, Compos. Sci. Technol. 102 (2014) 35–50.
- [4] G. Zhou, Y. Liu, L. He, Q. Guo, H. Ye, Microstructure difference between core and skin of T700 carbon fibers in heat-treated carbon/carbon composites, Carbon 49 (2011) 2883–2892.
- [5] Q. Wu, M. Li, Y. Gu, Z. Zhang, Nano-analysis on the structure and chemical composition of the interphase region in carbon fiber composite, Compos. Part A Appl. Sci. Manuf. (2014) 143–149.
- [6] J. Dong, C. Jia, M. Wang, X. Fang, H. Wei, H. Xie, T. Zhang, J. He, Z. Jiang, Y. Huang, Improved mechanical properties of carbon fiber-reinforced epoxy composites by growing carbon black on carbon fiber surface, Compos. Sci. Technol. 149 (2017) 75–80.
- [7] G.J. Ehlert, U. Galan, H.A. Sodano, Role of surface chemistry in adhesion between ZnO nanowires and carbon fibers in hybrid composites, ACS Appl. Mater. Interfaces 5 (2013) 635–645.
- [8] D.P. Cole, T.C. Henry, F. Gardea, R.A. Hynes, Interphase mechanical behavior of carbon fiber reinforced polymer exposed to cyclic loading, Compos. Sci. Technol. 151 (2017) 202–210.
- [9] F. Zhao, Y. Huang, Grafting of polyhedral oligomeric silsesquioxanes on a carbon fiber surface: novel coupling agents for fiber/polymer matrix composites, J. Mater. Chem. 21 (2011) 3695.

[10] D.J. Eyckens, D.J. Hayne, T.R. Walsh, F. Stojcevski, A. Hendlmeier, J.D. Randall, M.K. Stanfield, B. Newman, F. Vukovic, L.C. Henderson, Carbon fibre surface chemistry and its role in fibre- to-matrix adhesion, J. Mater. Chem. 9 (2021), 26538

- [11] Y.C. Chiou, H.Y. Chou, M.Y. Shen, Effects of adding graphene nanoplatelets and nanocarbon aerogels to epoxy resins and their carbon fiber composites, Mater. Des. 178 (2019), 107869.
- [12] A.K. Pathak, M. Borah, A. Gupta, T. Yokozeki, S.R. Dhakate, Improved mechanical properties of carbon fiber/graphene oxide-epoxy hybrid composites, Compos. Sci. Technol. 135 (2016) 28–38.
- [13] C. Wang, J. Li, J. Yu, S. Sun, X. Li, F. Xie, B. Jiang, G. Wu, F. Yu, Y. Huang, Grafting of size-controlled graphene oxide sheets onto carbon fiber for reinforcement of carbon fiber/epoxy composite interfacial strength, Compos. Part A 101 (2017) 511, 520.
- [14] J.D. Randall, F. Stojcevski, N. Djordjevic, A. Hendlmeier, B. Dharmasiri, M. K. Stanfield, D.B. Knorr, N.T. Tran, R.J. Varley, L.C. Henderson, Carbon fiber polypropylene interphase modification as a route to improved toughness, Compos. Part A. 159 (2022), 107001.
- [15] X. Han, Y. Huang, S. Gao, G. Zhang, T. Li, P. Liu, A hierarchical carbon fiber@ MXene@ZnO core-sheath synergistic microstructure for efficient microwave absorption and photothermal conversion, Carbon 183 (2021) 872–883.
- [16] Y. Zhu, S. Murali, W. Cai, X. Li, J.W. Suk, J.R. Potts, R.S. Ruoff, Graphene and graphene oxide: synthesis, properties, and applications, Adv. Mater. 22 (2010) 3906–3924.
- [17] A. Lipatov, H. Lu, M. Alhabeb, B. Anasori, A. Gruverman, Y. Gogotsi, A. Sinitskii, Elastic properties of 2D Ti₂C₂T_x MXene monolayers and bilayers, Sci. Adv. 4 (2018), eaat0491.
- [18] Y. Sun, R. Ding, S.Y. Hong, J. Lee, Y.K. Seo, J.D. Nam, J. Suhr, MXene-xanthan nanocomposite films with layered microstructure for electromagnetic interference shielding and Joule heating, Chem. Engr. J. 410 (2021), 128348.
- [19] K. Hantanasirisakul, Y. Gogotsi, Electronic and optical properties of 2D transition metal carbides and nitrides (MXenes), Adv. Mater. 30 (2018), 1804779.
- [20] Y. Zhou, K. Maleski, B. Anasori, J.O. Thostenson, Y. Pang, Y. Feng, K. Zeng, C. B. Parker, S. Zauscher, Y. Gogotsi, J.T. Glass, C. Cao, Ti₃C₂T_x MXene-reduced graphene oxide compisite electrodes for stretchable supercapacitors, ACS Nano 14 (2020) 3576–3586.
- [21] T.S. Mathis, K. Maleski, A. Goad, A. Sarycheva, M. Anayee, A.C. Foucher, K. Hantanasirisakul, C.E. Shuck, E.A. Stach, Y. Gogotsi, Modified MAX phase synthesis for environmentally stable and highly conductive Ti₃C₂ MXene, ACS Nano 15 (4) (2021) 6420–6429.
- [22] M.C. Krecker, D. Bukharina, C.B. Hatter, Y. Gogotsi, V.V. Tsukruk, Bioencapsulated MXene flakes for enhanced stability and composite precursors, Adv. Funct. Mater. 30 (2020), 2004554.
- [23] Y. Hu, S. Pang, J. Li, J. Jiang, D.G. Papageorgiou, Enhanced interfacial properties of hierarchical MXene/CF composites via low content electrophoretic deposition, Compos. Part B 237 (2022), 109871.
- [24] J. Wu, J. Chen, Y. Zhao, W. Liu, W. Zhang, Effect of electrophoretic condition on the electromagnetic interference shielding performance of reduced graphene oxide-carbon fiber/epoxy resin composites, Compos. Part B 105 (2016) 167–175.
- [25] B. Gao, R. Zhang, M. He, L. Sun, C. Wang, L. Liu, L. Zhao, H. Cui, A. Cao, Effect of a multiscale reinforcement by carbon fiber surface treatment with graphene oxide/ carbon nanotubes on the mechanical properties of reinforce carbon/carbon composites, Compos. Part A 90 (2016) 433–440.
- [26] C. Wang, J. Li, S. Sun, X. Li, F. Zhao, B. Jiang, Y. Huang, Electrophoretic deposition of graphene oxide on continuous carbon fibers for reinforcement of both tensile and interfacial strength, Compos. Sci. Technol. 135 (2016) 46–53.
- [27] C.B. Hatter, A. Sarycheva, A. Levitt, B. Anasori, L. Nataraj, Y. Gogotsi, Electrically conductive MXene-coated glass fibers for damage monitoring in fiber-reinforced composites, C - J. Carbon Res. 6 (2020) 64.
- [28] M. Liu, Y. Zhou, A. Sarycheva, Y. Gogotsi, M. Bissett, R. Young, I. Kinloch, Deformation of and interfacial stress transfer in Ti₃C₂ MXene-polymer composites, ACS Appl. Mater. Interfaces 14 (8) (2022) 10681–10690.
- [29] S.L. Gao, E. M\u00e4der, S.F. Zhandarov, Carbon fibers and composites with epoxy resins: topography, fractography and interphases, Carbon 42 (2004) 515–529.
- [30] S. Nunna, M. Maghe, R. Rana, R.J. Varley, D.B. Knorr Jr., J.M. Sands, C. Creighton, L.C. Henderson, M. Naebe, Time dependent structure and property evolution in fibres during continuous carbon fibre manufacturing, Materials 12 (2019) 1069.
- [31] K. Adstedt, F. Stojcevski, B. Newman, D.J. Hayne, L.C. Henderson, D. Mollenhauer, D. Nepal, V.V. Tsukruk, Carbon fiber surface functional landscapes: nanoscale topography and property distribution, ACS Appl. Mater. Interfaces 14 (2022) 4699–4713.
- [32] D.J. Eyckens, B. Demir, J.D. Randall, T.R. Gengenbach, L. Servinis, T.R. Walsh, L. C. Henderson, Using molecular entanglement as a strategy to enhance carbon fiberepoxy composite interfaces, Compos. Sci. Technol. 196 (2020), 108225.
- [33] M. Ghidiu, M.R. Lukatskaya, M.Q. Zhao, Y. Gogotsi, M.W. Barsoum, Conductive two-dimensional titatnium carbide 'clary' with high volumetric capacitance, Nature 516 (2014) 78.
- [34] M. Alhabeb, K. Maleski, B. Anasori, P. Lelyukh, L. Clark, S. Sin, Y. Gogotsi, Guidelines for synthesis and processing of 2D titanium carbide (Ti₃C₂T_x MXene), Chem. Mater. 29 (2017) 7633.
- [35] W.S. Hummers, R.E. Offeman, Preparation of graphitic oxide, J. Am. Chem. Soc. 80 (1958) 1339, 1339.
- [36] K. Hu, M.K. Gupta, D.D. Kulkarni, V.V. Tsukruk, Ultra-robust graphene-oxide silk firoin nanocomposite membranes, Adv. Mater. 25 (16) (2013) 2301–2307.

- [37] J. Wang, L. Liu, S. Jiao, K. Ma, J. Lv, J. Yang, Hierarchical carbon Fiber@MXene@ MoS2 core-sheath synergistic microstructure for tunable and efficient microwave absorption, Adv. Funct. Mater. 30 (2020), 2002595.
- [38] L. Liu, G. Ying, C. Hu, K. Zhang, F. Ma, L. Su, C. Zhang, Functionalization with MXene (Ti₃C₂) enhances the wettability and shear strength of carbon fiber-epoxy composites, ACS Appl. Nano Mater. 2 (2019) 5553–5562.
- [39] X. Zhao, A. Vashisth, E. Prehn, W. Sun, S.A. Shah, T. Habib, Y. Chen, Z. Tan, J. L. Lutkenhaus, M. Radovic, M.J. Green, Antioxidants unlock shelf-stable Ti₃C₂T_x (MXene) nanoflake dispersion, Matter 1 (2019) 512–526.
- [40] J. Halim, M.R. Lukatskaya, K.M. Cook, J. Lu, C.R. Smith, L.-A. Näslund, S.J. May, L. Hultman, Y. Gogotsi, P. Eklund, M.W. Barsoum, Transparent conductive twodimensional titatnium carbide epitaxial thin films, Chem. Mater. 26 (2014) 2374–2381
- [41] M.E. McConney, S. Singamaneni, V.V. Tsukruk, Probing soft matter with the atomic force microscopies: imaging and force spectroscopy, Polym. Rev. 50 (2010) 235–286
- [42] R.N. Youngworth, B.B. Gallagher, B.L. Stamper, An overview of power spectral density (PSD) calculations, in: Proc. SPIE 5869 Optical Manufacturing and Testing VI, 2005, p. 58690U, https://doi.org/10.1117/12.618478. Washington, USA.
- [43] B. Brück, T. Guglhoer, S. Haug, C. Kunzmann, M. Schulz, T. Schneck, J. Spoerl, M. R. Buchmeiser, S.R. Horn, W.M. Mueller, Surface characterization of carbon fibers by atomic force microscopy: roughness quantification by power spectral density, Key Eng. Mater. 742 (2017) 447–456.
- [44] https://www.nanophys.kth.se/nanolab/afm/icon/bruker-help/Content/SoftwareGuide/Offline/AnalysisFunct/Roughness.htm.
- [45] S.R.A. Brown, Note on the description of surface roughness using fractal dimension, Geophys. Res. Lett. 14 (11) (1987) 1095–1098.
- [46] S. Soumya, M.S. Swapna, V. Raj, V.P. Mahadevan Pillai, S. Sankararaman, Fractal analysis as a potential tool for surface morphology of thin films, Eur. Phys. J. Plus 132 (2017) 551.
- [47] B. Pittenger, N. Erina, C. Su, Quantitative Mechanical Property Mapping at the Nanoscale with Peakforce QNM. Bruker, 2010. http://www.cim.unipr.it/html/ PeakForce-ONM AFM AN128.pdf. (Accessed 2 October 2020).
- [48] U. Celano, Electrical Atomic Force Microscopy for Nanoelectronics, Springer-Nature, 2019.
- [49] C. Marcott, M. Lo, K. Kjoller, C. Prater, D.P. Gerrard, Applications of AFM-IR diverse chemical composiiton analyses at nanoscale spatial resolution, Microscopy Today 20 (6) (2012) 16–21.
- [50] F. Mohn, L. Gross, N. Moll, G. Meyer, Imaging the charge distribution within a single molecule, Nat. Nanotechnol. 7 (2012) 227–231.
- [51] T. Oldham, K. Simon, D.R. Ferriell, M.A. Belcher, A. Rubin, E. Thimsen, Highly uniform activation of carbon fiber reinforced thermoplastics by low-temperature plasma, ACS Appl. Polym. Mater. (2019) 2638–2648.
- [52] L. Fu, J. Zhou, L. Zhou, J. Yang, K. Wu, H. Zhao, J. Wang, K. Wu, Facile fabrication of exsolved nanoparticle-decorated hollow ferrite fibers as active electrocatalyst for oxygen evolution reaction, Chem. Eng. J. (Lausanne) 418 (2021), 129422.
- [53] J. Chen, K. Wang, Y. Zhao, Enhance interfacial interactions of carbon fiber reinforced PEEK composites by regulation PEI and graphene oxide complex sizing at the interface, Compos. Sci. Technol. 154 (2018) 175–186.
- [54] X. Zhao, Y. Che, Y. Mo, W. Huang, C. Wang, Fabrication of PEI modified GO/ MXene composite membrane and its application in removing metal cations from water, J. Membr. Sci. (2021) 640, 119847.
- [55] D.R. Dreyer, S. Park, C.W. Bielawski, R.S. Ruoff, The chemistry of graphene oxide, Chem. Soc. Rev. 39 (2010) 228–240.

- [56] J. Yun, I. Echols, P. Flouda, Y. Chen, S. Wang, X. Zhao, D. Holta, M. Radovic, M. J. Green, M. Naraghi, J.L. Lutkenhaus, Layer-by-layer assembly of reduced graphene oxide and MXene nanoflakes for wire-shaped flexible supercapacitors, ACS Adv. Mater. Inter. 13 (12) (2021) 14068–14076.
- [57] Y. Hu, S. Pang, G. Yang, X. Yao, C. Li, J. Jiang, Y. Li, MXene modified carbon fiber composites with improved mechanical properties based on electrophoretic deposition, Mater. Res. Bull. 150 (2022), 111761.
- [58] J. Chen, J. Wu, H. Ge, D. Zhao, C. Liu, X. Hong, Reduced graphene oxide deposited carbon fiber reinforced polymer composites for electromagnetic interference shielding, Compos. Part A 82 (2016) 141–150.
- [59] A.M. Navarro-Suárez, K. Maleski, T. Makaryan, J. Yan, B. Anasori, Y. Gogotsi, 2D titanium carbide/reduced graphene oxide heterostructures for supercapacitor applications, Batteries & Supercaps 1 (2018) 33–38.
- [60] N. Zheng, J. He, J. Gao, Y. Huang, F. Besenbacher, M. Dong, Adhesion force measured by atomic force microscopy for direct carbon fiber-epoxy interfacial characterization, Mater. Des. 145 (2018) 218–225.
- [61] M.S. Al-Haik, M.Y. Hussain, Molecular dynamic simulations of magnetic field induced orientation of nanotube-polymer composite, Japan. J. Appl. Phys. Part 1—Regular Pap. Brief Commun. Rev. Pap. 45 (2006) 8984–8987.
- [62] C. Wang, J. Li, S. Sun, X. Li, F. Zhao, B. Jiang, Y. Huang, Electrophoretic deposition of graphene oxide on continuous carbon fibers for reinforcement of both tensile and interfacial strength, Compos. Sci. Technol. 135 (2016) 46–53.
- [63] D. Wang, S. Fujinami, K. Nakajima, S. Inukai, H. Ueki, A. Magario, T. Noguchi, M. Endo, T. Nishi, Visualization of nanomechanical mapping on polymer nanocomposites by AFM force measurement, Polymer 51 (2010) 2455–2459.
- [64] H.S. Bedi, M. Tiwaei, P.K. Agnihotri, Quantitative determination of size and properties of interphases in carbon nanotube-based multiscale composites, Carbon 132 (2018) 181–190.
- [65] Y. Qi, D. Jiang, S. Ju, J. Zhang, X. Cui, Determining the interphase thickness and properties in carbon fiber reinforced fast and conventional curing epoxy matrix composites using peak force atomic forec microscopy, Compos. Sci. Technol. 184 (2019), 107877.
- [66] R. Oliwa, M. Heneczkowski, J. Oliwa, M. Olesky, Mechanical strength of epoxy/ organoclay/carbon fiber hybrid composites, Polym. J. 62 (2017) 658–665.
- [67] Z. Wen, X. Qian, Y. Zhang, X. Wang, W. Wang, S. Song, Electrochemical polymerization of carbon fibers and its effect on the interfacial properties of carbon reinforced epoxy resin composites, Composites Part A 119 (2019) 21–29.
- [68] P. Li, p. Li, Structure and performance analysis of new carbon nanomaterials based on microscopic imaging technology, Acta Microscopia 29 (4) (2020) 1832–1838.
- [69] T. Schultz, N. Frey, K. Hantanasirisakul, S. Park, S.J. May, V. Shenoy, Y. Gogotsi, N. Koch, Surface termination dependent work function and electronic properties of Ti₃C₂T_x MXene, Chem. Mater. 31 (17) (2019) 6590–6597.
- [70] T. Busolo, D.P. Ura, S.K. Kim, M. Marzec, A. Bernasik, U. Stachewicz, S. Kar-Narayan, Surface potential tailoring of PMMA fibers by electrospinning for enhanced triboelectric performance, Nano Energy 57 (2019) 500–506.
- [71] D. Nepal, S. Kang, K.M. Adstedt, K. Kanhaiya, M.R. Bockstaller, L.C. Brinson, M. J. Buehler, P.V. Coveney, K. Dayal, J.A. El-Awady, L.C. Henderson, D.L. Kaplan, S. Keten, N.A. Kotov, G.C. Schatz, S. Vignolini, F. Vollrath, B.I. Yacobson, V. V. Tsukruk, H. Heinz, New frontiers of structural bioinspired nanocomposites: advances and opportunities, Nat. Mater. (2022) in press.
- [72] S.J. Pety, M.H.Y. Tan, A.R. Najafi, P.R. Barnett, P.H. Geubelle, S.R. White, Carbon fiber composites with 2D microvascular networks for battery cooling, Int. J. Heat Mass Tran. 115 (2017) 513–522.